NANO · MICRO small
www.small-journal.com

Orthogonal Light-Dependent Membrane Adhesion Induces Social Self-Sorting and Member-Specific DNA Communication in Synthetic Cell Communities

Ali Heidari, Oya I. Sentürk,* Shuo Yang,* Alex Joesaar,* Pierangelo Gobbo,* Stephen Mann,* Tom F. A. deGreef,* and Seraphine V. Wegner**

Developing orthogonal chemical communication pathways in diverse synthetic cell communities is a considerable challenge due to the increased crosstalk and interference associated with large numbers of different types of sender-receiver pairs. Herein, the authors control which sender-receiver pairs communicate in a three-membered community of synthetic cells through red and blue light illumination. Semipermeable protein-polymer-based synthetic cells (proteinosomes) with complementary membrane-attached protein adhesion communicate through single-stranded DNA oligomers and synergistically process biochemical information within a community consisting of one sender and two different receiver populations. Different pairs of red and blue light-responsive protein-protein interactions act as membrane adhesion mediators between the sender and receivers such that they self-assemble and socially self-sort into different multicellular structures under red and blue light. Consequently, distinct sender-receiver pairs come into the signaling range depending on the light illumination and are able to communicate specifically without activation of the other receiver population. Overall, this work shows how photoswitchable membrane adhesion gives rise to different self-sorting protocell patterns that mediate member-specific DNA-based communication in ternary populations of synthetic cells and provides a step towards the design of orthogonal chemical communication networks in diverse communities of synthetic cells.

1. Introduction

Intercellular communication is essential to coordinate the collective operation of individual cells and to establish multicellular structures with specialized cells.[1,2] For this, sender cells secrete signals in the form of diffusible chemicals which can be recognized by receiver cells within the signaling range and with appropriate receptors. Building similar capabilities into synthetic cells allows community-based functions and interactions among synthetic cells[3,4] and living cells.[5] Remarkable achievements of communication in synthetic cells include communities that process DNA-coded information through reaction networks,[6] mimic quorum sensing,[7,8] differentiate into different patterns,[9] exhibit prey-predatory relationships,[10] synchronization,[11] and oscillations,[12,13] and regulate cellular behavior in response to physiological conditions.[14] These studies illustrated how communication in synthetic cells helps to understand underlying organizational

A. Heidari, S. V. Wegner
Institute of Physiological Chemistry and Pathobiochemistry
University of Münster
Waldeyerstr. 15, 48149 Münster, Germany
E-mail: heidaria@uni-muenster.de; wegnerse@exchange.wwu.de

O. I. Sentürk
Department of Physical Chemistry of Polymers
Max Planck Institute for Polymer Research
Ackermannweg 10, 55128 Mainz, Germany
E-mail: sentuerk@mpip-mainz.mpg.de

The ORCID identification number(s) for the author(s) of this article can be found under https://doi.org/10.1002/smll.202206474.

DOI: 10.1002/smll.202206474

S. Yang, A. Joesaar, T. F. A. Greef
Laboratory of Chemical Biology and Institute for Complex Molecular Systems
Department of Biomedical Engineering
Eindhoven University of Technology
Eindhoven 5612 AZ, The Netherlands
E-mail: yangshuo19870414@gmail.com; A.H.Joesaar@tudelft.nl; t.f.a.d.greef@tue.nl

P. Gobbo
Department of Chemical and Pharmaceutical Sciences
University of Trieste
Trieste 34127, Italy
E-mail: pierangelo.gobbo@units.it

S. Mann
Centre for Protolife Research and Centre for Organized Matter Chemistry
Max Planck Bristol Centre for Minimal Biology
School of Chemistry
University of Bristol
Bristol BS8 1TS, UK
E-mail: s.mann@bristol.ac.uk

principles, program multicellular communities towards new applications, and interface synthetic cells with living ones.[15,16]

Communication between synthetic cells depends on the spatiotemporal distribution of the signaling molecule, which is affected by the local densities of sender and receiver cells and the production, release, propagation, degradation, and consumption rates of the signal.[17] In synthetic sender cells with a limited signal reservoir, the signaling range is limited to the direct neighborhood after which the signal is diluted below its effective concentrations.[4] Consequently, the spatial organization of the sender and receiver is critical for the perception of the signal.[18,19] Prominent examples of such short-range communication in biology include the neurotransmitters that signal within the neural network and different immune cells that adhere to each other for effective exchange.[20,21] In synthetic cell communities, senders and receivers can be placed within signaling range with microfluidic techniques,[22] acoustic waves,[23] or optical tweezers.[24] In addition, the direct adhesions between synthetic cells give rise to the self-assembly of large multiprotocellular structures and regulate signal exchange in bulk solution.[25,26]

The number of different cell types is an important characteristic of a community to consider as the number of possible binary relationships increases rapidly with the increasing number of cell types ($[n^2 - n]/2$). Therefore, in diverse synthetic cell communities, the specificity of communication between different pairs becomes a concern and this is why most studies are limited to two-membered communities. Biology has solved the problem of specificity through the spatial distribution of senders and receivers in short-range paracrine signaling, which provides a principle that can also be implemented with synthetic cells.[25] When more than two different types of cell-sized microscale objects (e.g., colloids) are mixed, multiple possibilities of spatial arrangement are conceivable along with different self-sorting patterns that arise from the specificity of the surface interactions. In mixtures, specific homophilic adhesions between colloids result in narcissistic self-sorting, where each member of the community forms its own sub-assemblies.[27,28] In contrast, specific heterophilic interactions result in social self-sorting, where domains with two member types emerge but other populations are excluded.[28,29] Following similar principles different cell types are sorted into different cell layers during early embryonic development.[30]

The self-assembly and self-sorting of dispersed synthetic cells require specific and non-interfering (orthogonal) interactions between different populations in response to distinct stimuli. Here, we demonstrate how social self-sorting and communication can be dynamically regulated in a three-membered community of synthetic cells. The community is composed of one sender and two potential receivers and can be socially self-sorted into different structures under either red or blue light. Depending on the illumination conditions, a different receiver cell comes into the signaling range of the sender protocell and perceives the liberated chemical signal. Towards this goal, we use two pairs of light-dependent heterophilic protein-protein interactions to induce selective adhesions and social self-sorting of semipermeable protein-polymer-based synthetic cells (proteinosomes).[31] The protein-protein interactions are triggered with different colors of light, determined by photo-induced conformational changes that open up specific binding sites for the cognate binding partner. In this paper, we employ red light for the binding of the proteins PhyB and PIF6,[32] and blue light for the binding of the proteins iLID and Nano.[33] In each case, protein binding requires only low intensities of light and is accomplished in buffered solutions. Given these properties, we couple the light-responsive proteins to the outer surface of different proteinosomes to produce a community of synthetic cells with complementary membrane-attached adhesion mediators that when initiated results in self-sorting and define chemical communication. We employ a signaling pathway based on a previously reported DNA-based protocell programming network (biomolecular implementation of protocellular communication, BIO-PC), where different proteinosomes communicate through distributed DNA strand displacement (DSD) reactions.[17,22] DSD cascade reactions are highly programmable and utilizing sequence-specific DNA gates can code for functions such as oscillations,[34] digital logic circuits,[35,36] and Boolean neural networks.[37] Taken together, our work exemplifies, how the multicolor light regulation of organization in three-membered communities of synthetic cells dictates the outcome of chemical communication.

2. Results

To functionalize the proteinosome membrane with photoswitchable proteins capable of acting as adhesion mediators, we prepared proteinosomes decorated with Ni^{2+}-NTA (nitrilotriacetic acid) so that proteins with a polyhistidine tag (His-tag) could be immobilized on the outer surface of the synthetic cells. The proteinosomes were prepared by adapting a previously reported three-step protocol.[31] In short, protein-polymer conjugates were synthesized by reacting the primary amines of cationized bovine serum albumin (BSA-NH_2, labeled with Rhodamine B for fluorescence microscopy visualization of the proteinosomes) with the mercaptothiazoline-activated terminal amide of poly *N*-isopropyl acrylamide (PNIPAM). In addition, 1% of the PNIPAM sidechains contained NTA functionalities (PNIPAM-co-NTA) (Scheme S1, and Figures S1—S9, Supporting Information, characterization through ^1H and ^{13}C NMR, FT-IR and MALDI spectroscopy, determination of LCST, zeta potential and hydrodynamic diameter). Subsequently, the proteinosomes were formed by the interfacial assembly of the protein-polymer conjugates at the water droplet/oil interface of a Pickering emulsion. The conjugates were then cross-linked and the proteinosomes were transferred to the water phase (Figure S10, Supporting Information). The NTA groups on the resultant proteinosomes were subsequently loaded with Ni^{2+} ions. To demonstrate that the Ni^{2+}-NTA groups on the surface are accessible, we incubated the proteinosomes with the His-tagged fluorescent protein, miCy. We observed bright miCy fluorescence for proteinosomes with Ni^{2+}-loaded NTA groups but control proteinosomes that were not loaded with Ni^{2+} were not fluorescent (Figure S11, Supporting Information). The surface density of His-tagged proteins on the proteinosomes was $\Gamma = 4949\,\mu m^{-2}$ (Figure S11D,E, Supporting Information), which was determined by comparing the fluorescence intensity from His-tagged GFP on the periphery of proteinosomes and

giant unilamellar vesicles with 1% Ni^{2+}-NTA containing lipids known lipid packing.[38] In addition, we determined in ssDNA uptake measurements that functionalization with His-tagged proteins did not change the membrane permeability of the proteinosomes (Figure S12, Supporting Information). The results indicated that the binding of His-tags to Ni^{2+}-NTA groups is a reliable method for attaching auxiliary proteins to the outer surface of the proteinosome membrane; thus, in all subsequent experiments, the proteinosomes were functionalized with the desired His-tagged proteins.

To control the self-assembly of two-membered communities of proteinosomes with adhesions that are triggered independently using different colors of light, we co-functionalized potential sender (**S**) proteinosomes with PhyB and iLID proteins and two prospective receiver proteinosomes with either PIF6 (**R1**) or Nano (**R2**). When we mixed equal numbers of S and **R1** proteinosomes, the two types adhered to each other under red light but not in the dark or under blue light illumination (**Figure 1**A). On the other hand, mixtures of the **S** and **R2** proteinosomes only aggregated under blue light and not in the dark or under red light illumination (Figure 1B). The adhesions between the **S** and **R** proteinosomes led to membrane deformations and large contact sides (Figures S13 and S14, Supporting Information). Moreover, we quantified the aggregation ratio (area of objects larger than 2000 μm^2/area of all objects) of these proteinosome mixtures after 90 min shaking on a 2D shaker at 30 rpm with different illumination conditions. (Appropriate shaking was important to increase the likelihood of the proteinosomes coming into contact; however, too high shear forces can also disrupt the aggregates).[39] For the S:R1 mixture, the proteinosome aggregation ratio was about four times higher under red light illumination than under dark or blue light illumination (**Figure 1**C). Similarly, for the S:R2 mixture the aggregation ratio was two-fold higher under blue light than in the dark or under red light. As proteinosomes have a broad size distribution (diameter = 10–70 µm, median = 20 µm, area = 79–3850 μm^2, median = 314 μm^2) (Figure S15, Supporting Information), the aggregation ratio only takes into account large clusters (>2000 μm^2) to avoid counting large single proteinosomes. Consequently, this method disregards clusters composed of multiple small proteinosomes. Despite underestimating the aggregation ratio, the extent of proteinosome aggregation was above 50% for S:R1 and S:R2 mixtures under red and blue light, respectively. Overall, the results showed that membrane-bounded photoswitchable protein pairs PhyB/PIF6 and iLID/Nano are suitable to induce the contact-dependent adhesion of proteinosomes when exposed to specific wavelengths of light.

To illustrate how the communication in synthetic cells can be modulated through the light-controlled proximity of S and R proteinosomes, we distributed different steps of the DSD cascade reaction between the two populations.[22] In our design, the S-type proteinosomes contained a DNA gate complex F1Q1, where the biotinylated F1 strand was labeled with an Alexa488 fluorophore (1.3 µM) and anchored to a streptavidin (15 µM) (Figures S16 and S17, Supporting Information), and the Q1 strand acted as a fluorescence quencher when hybridized with F1 (**Figure 2**A). The R-type proteinosomes were loaded with

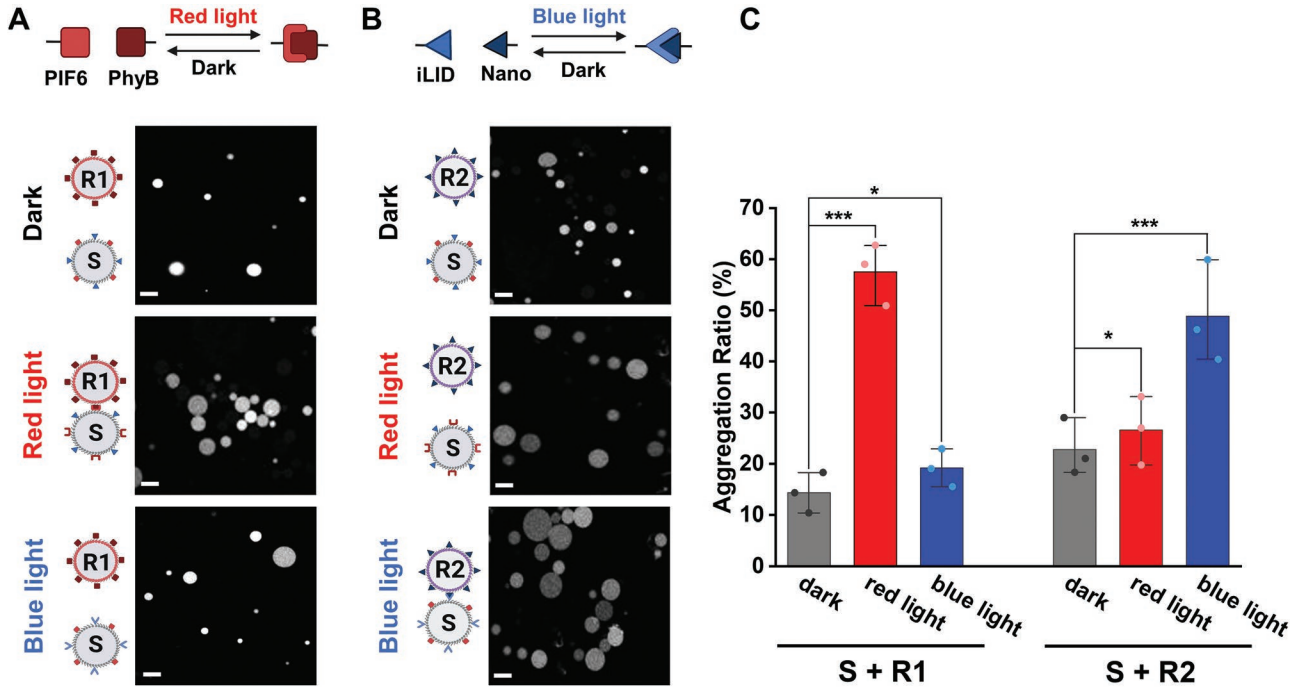

Figure 1. Red or blue light controlled aggregation in two membered proteinosome communities. Fluorescence confocal microscopy images of S proteinosomes functionalized with PhyB and iLID and mixed with A) PIF6 functionalized R1 proteinosomes or B) Nano functionalized R2 proteinosomes in the dark, under red light or under blue light after 90 min incubation. S and R1 aggregate under red light due to the red light-triggered binding of PhyB and PIF6. S and R2 adhere to each other under blue light due to the blue light-dependent binding of iLID and Nano. Scale bars are 30 µm. C) Aggregation ratio of S:R1 and S:R2 proteinosome mixtures under different conditions. Error bars are the standard error of the mean from three independent experiments with > 50 proteinosomes per sample.

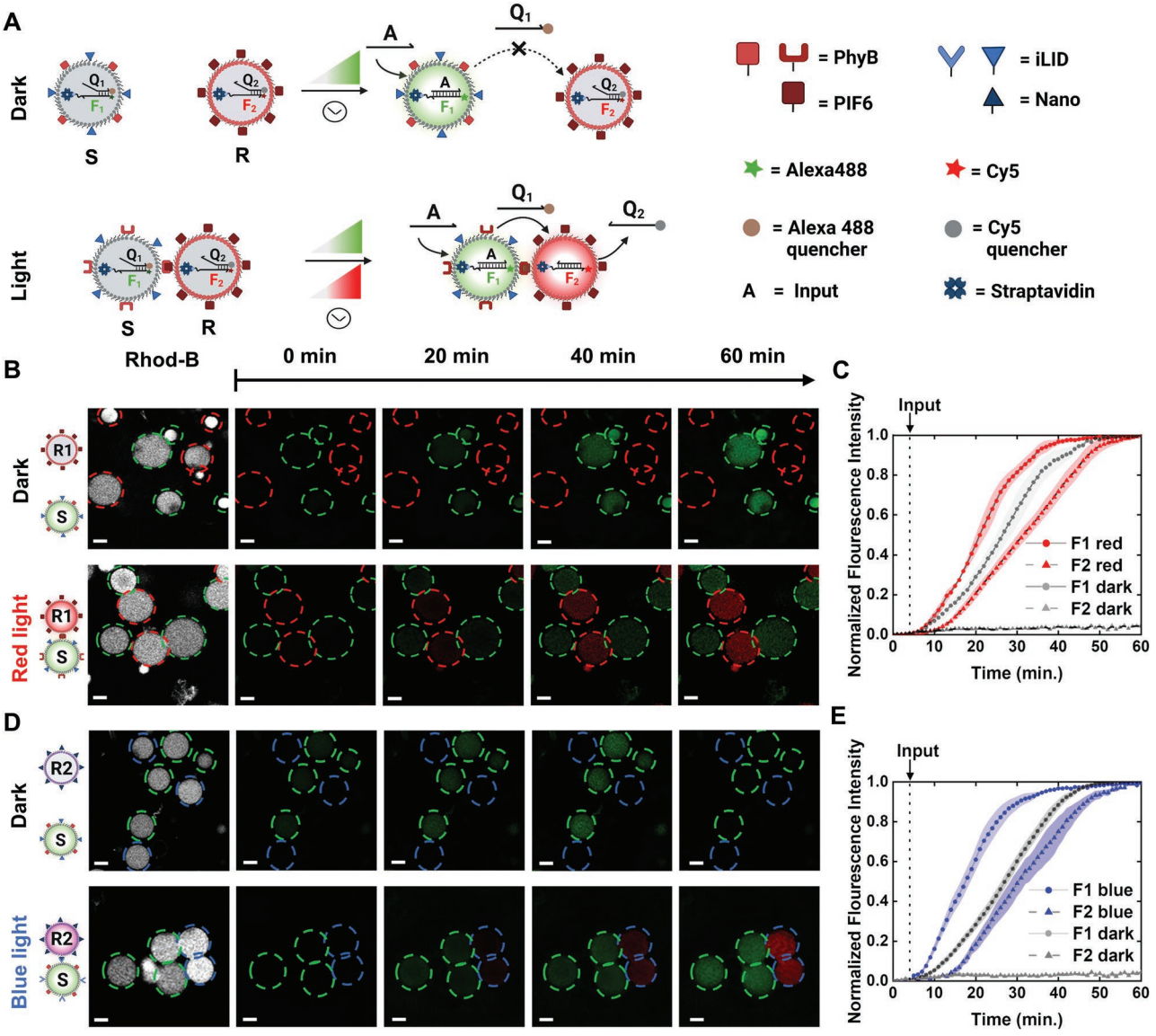

Figure 2. Light-regulated proximity controls communication between sender and receiver proteinosomes. A) S-type proteinosomes loaded with F1Q1 DNA gate complex release Q1 and exhibit an increase in Alexa488 green fluorescence upon the addition of the input strand *A* in the first step of the DSD cascade. In the dark, R-type proteinosomes are too far from S-type proteinosomes and do not receive the Q1 signal. Under the light of appropriate wavelength, S- and R-type proteinosomes are in close proximity, and Q1 displaces the Q2 strand from the F2Q2 DNA gate complex, resulting in an increase in Cy5 red fluorescence. B,D) Confocal microscopy images recorded in Rhod-2 (white), Alexa488 (green), and Cy5 (red) channels of S (circled in green) with R1 (circled in red) or R2 (circled in blue) proteinosomes (S:R ratio 1:1) in the dark and under red or blue light illumination, respectively, after 90 min prior incubation. Strand *A* is then added at t = 0 min. The scale bars are 20 µm. C,E) Normalized fluorescence intensity of Alexa488 in S (F1 strand) and Cy5 on R (F2 strand) proteinosomes. The fluorescence of individual proteinosomes ($n > 45$) in three independent experiments was measured and the error bars are the standard error of the mean.

an F2Q2 DNA gate complex, where the streptavidin-anchored F2 strand was labeled with Cy5 and Q2 with a corresponding quencher. The DSD reaction cascade was designed such that in the first step the addition of an ssDNA input strand (*A*) displaces Q1 from the F1Q1 complex, resulting in an increase in Alexa488 fluorescence in **S** and the concomitant release of Q1 as a diffusive chemical signal. In the second step, if the Q1 signal reaches an R proteinosome, displacement of the Q2 strand from the F2Q2 complex gives rise to an increase in Cy5 fluorescence in **R**. Notably, given that the S proteinosomes can only release a limited amount of signal (Q1 strand), only R type proteinosomes in their direct neighborhood where the local signal is high enough can respond. The release profile of the Q1 strand from the **S** proteinosomes with different sizes (diameter, 30–70 µm), showed that at a distance of 5 µm from the membrane the concentrations diluted to the background level (Figure S18, Supporting Information), which corresponds to a signaling range below the average size of a proteinosome.

To demonstrate how the proximity of sender and receiver proteinosomes regulates the selective chemical communication

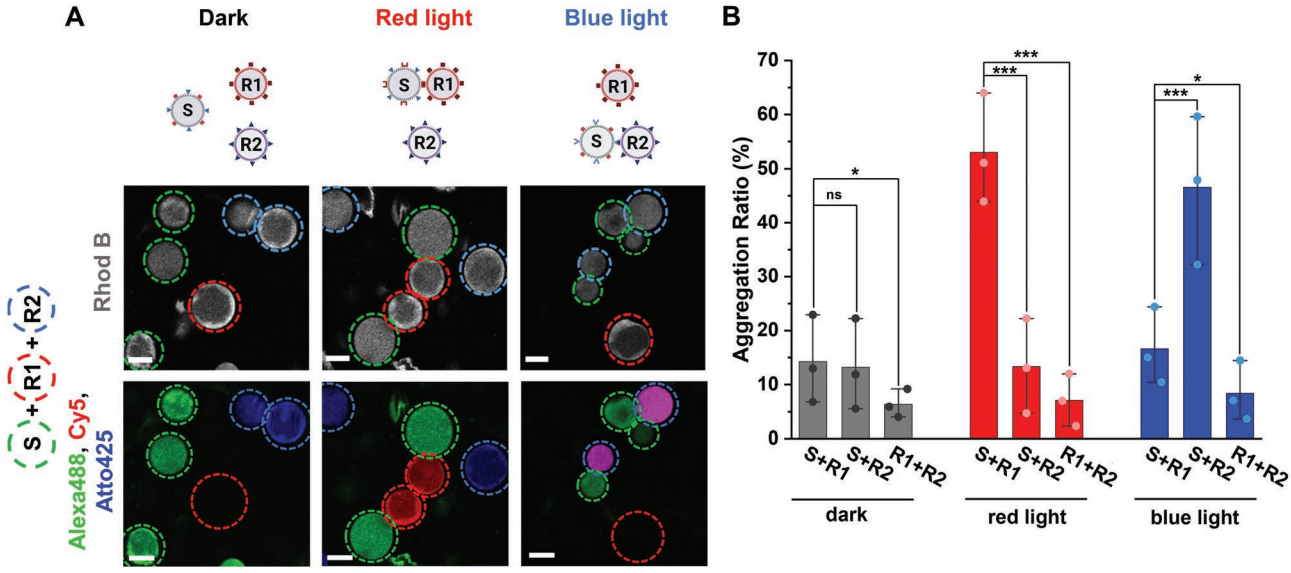

Figure 3. Orthogonal social self-sorting with red and blue light in three-membered synthetic cell communities. A) Confocal microscopy images of S, R1, and R2 proteinosomes (2:1:1 ratio) after 90 min incubation under different illumination conditions. While all proteinosomes remain dispersed in the dark, S and R1 adhere under red light due to membrane PhyB-PIF6 binding; in contrast, S and R2 adhere under blue light due to iLID-Nano binding. The scale bars are 20 µm. B) Aggregation ratio between different pairs in the three-membered communities under different illumination conditions. Error bars are the standard error of the mean from three independent experiments with > 100 proteinosomes per sample.

between synthetic cells, we controlled the average inter-protocell spacing through photoswitchable adhesions (Figure 2A). For this, equal numbers of S- and R- type proteinosomes were mixed and incubated for 90 min either in the dark or under red (**S:R1**) or blue (**S:R2**) light (Figure 2B,D). In illuminated samples, the S and R populations formed clusters but remained dispersed in the dark. Subsequent addition of the input strand *A* to the bulk solution initiated the first step of the DSD cascade, which was visible as an increase in Alexa488 green fluorescence inside the S-type proteinosomes. The increase in fluorescence took place in the dark and under light illumination. In contrast, the second step of the DSD cascade, as evidenced by an increase in Cy5 fluorescence in the R-type proteinosomes, only took place under red light illumination in S:R1 and under blue light illumination in S:R2 populations. The population-level quantification of the two DSD reactions over time in the two-membered communities showed that for the first step of the DSD reaction, the increase in Alexa488 fluorescence reached a maximum over time both in the dark and under light, which shows the finite capacity of S to produce the soluble signal (Figure 2C,E). In addition, the Cy5 output of the second DSD reaction emerged with a time delay compared to the Alexa488 signal in the illuminated samples (Figure 2C,E), confirming the sequence of events in the communication pathway. Overall, the results show that molecular communication between the proteinosomes depends on the spatial connectivity of the proteinosomes, which can be tuned with red or blue light illumination.

Given the above observations, we sought to demonstrate light-directed social self-sorting behavior as a mechanism for regulating the chemical communication pathways in three-membered synthetic cell communities composed of one sender and two receiver populations. To achieve this, we mixed S-, R1-, and **R2**-type proteinosomes in a 2:1:1 ratio and analyzed their self-sorting under different illumination conditions (**Figure 3**A). As above, the proteinosomes were membrane-functionalized with the respective proteins (S: PhyB and iLID, R1:PIF6, and **R2**:Nano) and housed the components of the DSD cascade reaction (F1Q1 in **S**, F2Q2 in **R1** and F2Q2 in **R2**). The **R2**-type proteinosomes also contained an additional Atto425-biotin label to distinguish between the **R1** and **R2** populations. In the dark, the three types of proteinosomes remained dispersed in the solution. Under red light, the S and **R1** type proteinosomes adhered selectively due to membrane-based PhyB-PIF6 interactions, while the **R2** type proteinosomes remained separated. In contrast, under blue light, the S and **R2** proteinosomes bound to each other due to the iLID-Nano interactions and the **R1** type proteinosomes remained detached. We further analyzed the aggregation ratios of different pairs to confirm orthogonal social self-sorting in the three-membered community (Figure 3B). In the dark, none of the paired interactions, S:R1, S:R2, and R1:R2 showed significant aggregation ratios. In contrast, high aggregation ratios were observed for either the S:R1 or S:R2 pairs after exposure to red or blue light, respectively. Moreover, the constantly low aggregation ratio of the R1:R2 pair independent of the illumination condition and the low S:R1 and S:R2 aggregation under blue and red light, respectively, indicated the low extent of non-specific interactions between the receiver proteinosomes. Taken together, the results indicate that the social self-sorting of **S:R1 and S:R2** pairs in three-membered communities can be triggered independently from each other without interference.

Having established selective sorting behavior, we sought to regulate the specificity of the communication pathway through the photo-triggering of spatial organization in three-membered synthetic communities. For this, we added the input ssDNA strand to the ternary population described above and observed

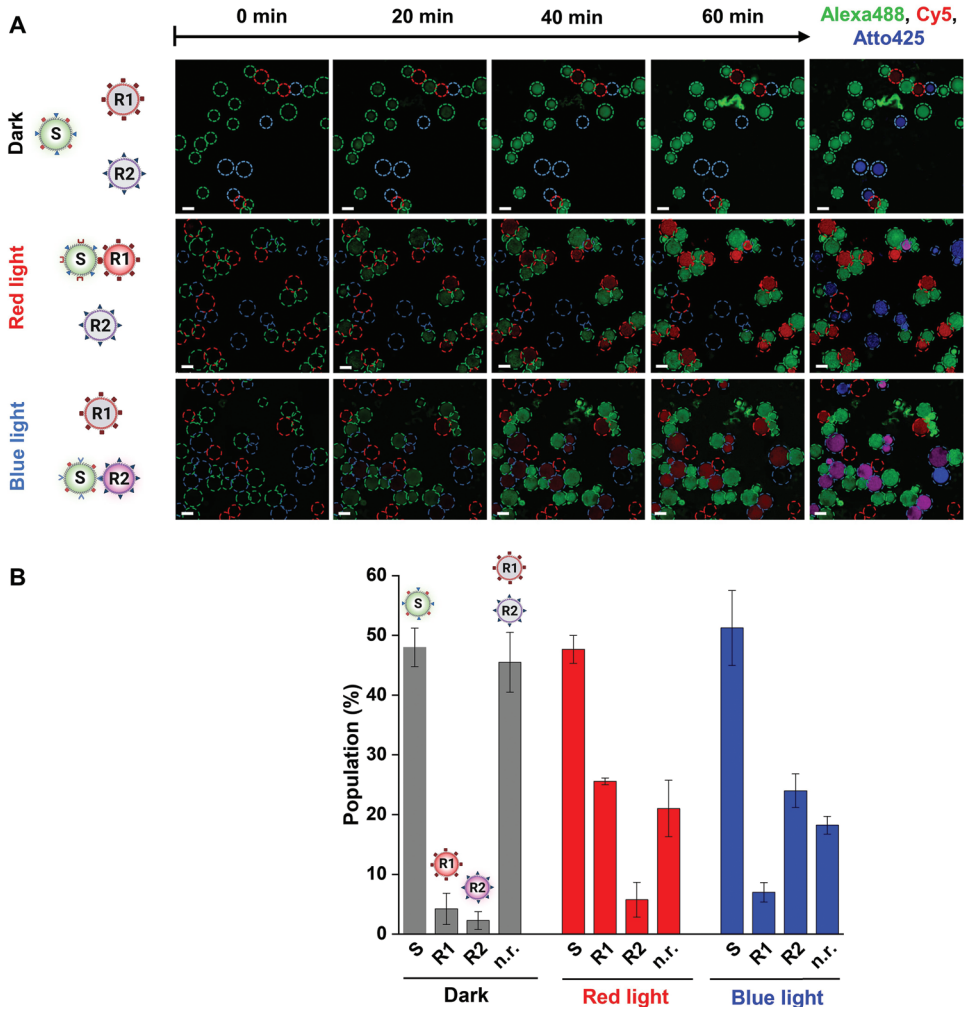

Figure 4. Specific DNA-based communication through different social sorting patterns in three-membered proteinosome communities. A) Confocal microscopy images of mixtures of S, R1, and R2 type proteinosomes (2:1:1 ratio) in the dark and under red or blue light illumination, respectively, after 90 min prior incubation. The ssDNA input strand, *A*, was added at $t = 0$ min. Alexa488 (green, release of signal strand), Cy5 (red, release of output strand), and Atto425 (blue, identification label) were used to identify S (circled in green), R1 (circled in red), and R2 (circled in blue). While essentially all S proteinosomes increased in Alexa488 fluorescence, only R1 and R2 increased in Cy5 fluorescence under red and blue light, respectively. Purple coloration in R2 proteinosomes is due to the overlay of Cy5 and Atto425 fluorescence. Non-responders were identified from fluorescence images recorded in the rhodamine B (proteinosome membrane label) channel. The scale bars are 50 µm. B) Bar chart showing population percentage of S, activated R1, activated R2, and non-responders (n.r) under different conditions in (B). Error bars are the standard error of the mean from three independent experiments with >50 proteinosomes per sample.

that the S-type proteinosomes increased in Alexa488 green fluorescence due to the release of the Q1 strand in the first step of the DSD cascade (**Figure 4**A). In the dark, the proteinosomes remained dispersed and the levels of released Q1 strand were unfunctional due to dilution in the bulk phase; thus, no increase in Cy5 red fluorescence was detected in the **R1** or **R2** type proteinosomes (Figure 4A). On the other hand, under red light illumination, the Q1 strand reached the attached **R1** type proteinosomes, resulting in an increase in Cy5 red fluorescence and indicating successful signal transfer and release of strand Q2 from the **R1** (Figure 4A). Conversely, under blue light illumination, Cy5 red fluorescence increased in the **R2** population (Figure 4A). To demonstrate that the lack of response in **R1 or R2** type proteinosomes was due to the limited local concentrations of Q1 strand released from the S-type proteinosomes and not due to a lack of functionality in the receivers, we added an external excess of Q1 to the community in the dark and observed that both **R1** and **R2** type proteinosomes increased in Cy5 fluorescence, confirming their latent activity (Figure S19, Supporting Information).

We quantified the communication response in the three-membered community under different illumination conditions (Figure 4B). Under all conditions (dark, red light, and blue light), the presence of Alexa488 green fluorescence was associated with ≈50% of the total population, consistent with the activation of essentially all the S-type proteinosomes in a community prepared with an initial S:R1:R2 mixing ratio of 2:1:1. In the dark, about 50% of the population were none-responders (no Cy5 output), with less than 5% of the **R1** and **R2** displaying an increase in Cy5 fluorescence, indicating a low level of

non-specific communication in the absence of light-mediated membrane-membrane adhesions. Under red light, the number of non-responders decreased to 20% and the number of activated **R2**-type proteinosomes remained at around 5%, but the number of activated **R1**-type proteinosomes increased to 25%. On the other hand, under blue light, the number of activated **R1**-type proteinosomes remained at ≈5% but the number of activated **R2**-type proteinosomes increased to 25%. Taken together, these results demonstrate that the distinct social self-sorting patterns of the different sender and receiver pairs under red and blue light lead to different specific communication outcomes.

3. Conclusion

In this paper, we demonstrated that specific communication pathways between different pairs of synthetic cells in mixed communities can be established through the spatial organization of different protocell types as long as the signaling range of the sender population is limited to nearest-neighbor interactions.[40] Different modes of self-sorting have been described for colloidal particles[27,28] and living cells[41] in the context of forming multicellular structures. Here, we show that the social self-sorting of proteinosome-based synthetic cells via selective membrane adhesion events can regulate DNA-based communication in a three-membered community. In particular, our results demonstrate that orthogonal self-sorting and independent photoswitchable triggering can be achieved using the high binding and light specificity of PhyB/PIF6 and iLID/Nano protein pairs. By preparing sender (S) proteinosomes with membranes decorated with both PhyB and iLID "receptors" different patterns of social self-sorting are achieved in the presence of receivers **R1** (PIF6) and **R2** (Nano) depending on the wavelength of light (red or blue, respectively) used to initiate sender-receiver membrane adhesion. Consequently, S to **R1** or S to **R2** communication pathways are established in the protocell community using a programmable DSD cascade in which the ssDNA diffusive signal released from **S** after activation is spatially limited. The orthogonality is maintained as long as the signaling range is restricted to distances below the dimension of a single protocell such that only directly adhered receivers are activated. This short-range effect is facilitated by turbulent mixing in the bulk solution, such that the ssDNA signal is only locally high enough to initiate a response close to its production site and becomes quickly diluted below a critical concentration at longer length scales. This is unlike previous studies using microfluidic chambers with the laminar flow or without any internal flow, where the sender-to-receiver signal only propagates by molecular diffusion. Thus, in contrast to other investigations, our approach offers high spatiotemporal control over the communication process in bulk solutions, without the need for immobilization of the protocells in hydrogels, fabricated chips, or microfluidic arrays.[22,42–44] In the long term, we expect the social self-sorting and highly programmable DSD-based communication pathways developed using our methodology to open up possibilities for the advent of diverse and interactive multi-protocellular communities and signaling networks.

Supporting Information

Supporting Information is available from the Wiley Online Library or from the author.

Acknowledgements

This work was funded by the European Research Council through the ERC Starting Grant ARTIST (#757593) and ERC Consolidator Grant AMIGA (#101000199). The authors thank Wilfried Weber and Maximilian Hörner from the University of Freiburg for providing the PhyB protein and Brian Kuhlman for the plasmids pQE-80L iLID (C530M) and pQE-80L MBP-SspB Nano (Addgene # 60408 and #60409).

Open access funding enabled and organized by Projekt DEAL.

Conflict of Interest

The authors declare no conflict of interest.

Data Availability Statement

The data that support the findings of this study are available from the corresponding author upon reasonable request.

Keywords

DNA-based communication, photoswitchable proteins, proteinosome, self-sorting, synthetic cells

Received: October 20, 2022
Revised: December 3, 2022
Published online: January 4, 2023

[1] J. T. Bonner, *Integr. Biol.* **1998**, *1*, 27.
[2] R. J. Wordinger, T. Sharma, A. F. Clark, *J. Ocul. Pharmacol. Ther.* **2014**, *30*, 154.
[3] J. M. Smith, R. Chowdhry, M. J. Booth, *Front. Mol. Biosci.* **2022**, *8*, 809945.
[4] L. Aufinger, F. C. Simmel, *Chem. – Eur. J.* **2019**, *25*, 12659.
[5] Y. Elani, *Angew. Chem., Int. Ed.* **2021**, *60*, 5602.
[6] A. S. Zadorin, Y. Rondelez, G. Gines, V. Dilhas, G. Urtel, A. Zambrano, J.-C. Galas, A. Estevez-Torres, *Nat. Chem.* **2017**, *9*, 990.
[7] K. Stephens, W. E. Bentley, *Trends Microbiol.* **2020**, *28*, 633.
[8] H. Niederholtmeyer, C. Chaggan, N. K. Devaraj, *Nat. Commun.* **2018**, *9*, 5027.
[9] J. W. Hindley, D. G. Zheleva, Y. Elani, K. Charalambous, L. M. C. Barter, P. J. Booth, C. L. Bevan, R. V. Law, O. Ces, *Proc. Natl. Acad. Sci. USA* **2019**, *116*, 16711.
[10] Y. Qiao, M. Li, R. Booth, S. Mann, *Nat. Chem.* **2017**, *9*, 110.
[11] S. Pérez-García, M. García-Navarrete, D. Ruiz-Sanchis, C. Prieto-Navarro, M. Avdovic, O. Pucciariello, K. Wabnik, *Nat. Commun.* **2021**, *12*, 4017.
[12] C. E. Hilburger, M. L. Jacobs, K. R. Lewis, J. A. Peruzzi, N. P. Kamat, *ACS Synth. Biol.* **2019**, *8*, 1224.
[13] T.-Y. D. Tang, D. Cecchi, G. Fracasso, D. Accardi, A. Coutable-Pennarun, S. S. Mansy, A. W. Perriman, J. L. R. Anderson, S. Mann, *ACS Synth. Biol.* **2018**, *7*, 339.
[14] A. Dupin, F. C. Simmel, *Nat. Chem.* **2019**, *11*, 32.

[15] O. Adir, M. R. Albalak, R. Abel, L. E. Weiss, G. Chen, A. Gruber, O. Staufer, Y. Kurman, I. Kaminer, J. Shklover, J. Shainsky-Roitman, I. Platzman, L. Gepstein, Y. Shechtman, B. A. Horwitz, A. Schroeder, *Nat. Commun.* **2022**, *13*, 2328.
[16] V. Mukwaya, S. Mann, H. Dou, *Commun. Chem.* **2021**, *4*, 161.
[17] S. Yang, P. A. Pieters, A. Joesaar, B. W. A. Bögels, R. Brouwers, I. Myrgorodska, S. Mann, T. F. A. de Greef, *ACS Nano* **2020**, *14*, 15992.
[18] X. Ren, G. Zhong, Q. Zhang, L. Zhang, Y. Sun, Z. Zhang, *Cell Res.* **2020**, *30*, 763.
[19] B. C. Buddingh', A. Llopis-Lorente, L. K. E. A. Abdelmohsen, J. C. M. van Hest, *Chem. Sci.* **2020**, *11*, 12829.
[20] Ö. D. Toparlak, J. Zasso, S. Bridi, M. D. Serra, P. Macchi, L. Conti, M.-L. Baudet, S. S. Mansy, *Sci. Adv.* **2022**, *6*, abb4920.
[21] I. Hwang, *Mol. Cells* **2013**, *36*, 105.
[22] A. Joesaar, S. Yang, B. Bögels, A. van der Linden, P. Pieters, B. V. V. S. P. Kumar, N. Dalchau, A. Phillips, S. Mann, T. F. A. de Greef, *Nat. Nanotechnol.* **2019**, *14*, 369.
[23] L. Tian, N. Martin, P. G. Bassindale, A. J. Patil, M. Li, A. Barnes, B. W. Drinkwater, S. Mann, *Nat. Commun.* **2016**, *7*, 13068.
[24] G. Bolognesi, M. S. Friddin, A. Salehi-Reyhani, N. E. Barlow, N. J. Brooks, O. Ces, Y. Elani, *Nat. Commun.* **2018**, *9*, 1882.
[25] T. Chakraborty, S. M. Bartelt, J. Steinkühler, R. Dimova, S. V. Wegner, *Chem. Commun.* **2019**, *55*, 9448.
[26] T. Chakraborty, S. V. Wegner, *ACS Nano* **2021**, *15*, 9434.
[27] O. I. Sentürk, E. Chervyachkova, Y. Ji, S. V. Wegner, *Small* **2019**, *15*, e1901801.
[28] K. Han, D. Go, T. Tigges, K. Rahimi, A. J. C. Kuehne, A. Walther, *Angew. Chem., Int. Ed.* **2017**, *56*, 2176.
[29] E. Chervyachkova, S. V. Wegner, *ACS Synth. Biol.* **2018**, *7*, 1817.
[30] S. Zhang, T. Chen, N. Chen, D. Gao, B. Shi, S. Kong, R. C. West, Y. Yuan, M. Zhi, Q. Wei, J. Xiang, H. Mu, L. Yue, X. Lei, X. Wang, L. Zhong, H. Liang, S. Cao, J. C. I. Belmonte, H. Wang, J. Han, *Nat. Commun.* **2019**, *10*, 496.
[31] X. Huang, M. Li, D. C. Green, D. S. Williams, A. J. Patil, S. Mann, *Nat. Commun.* **2013**, *4*, 2239.
[32] M. Hörner, K. Gerhardt, P. Salavei, P. Hoess, D. Härrer, J. Kaiser, J. J. Tabor, W. Weber, *ACS Synth. Biol.* **2019**, *8*, 2442.
[33] G. Guntas, R. A. Hallett, S. P. Zimmerman, T. Williams, H. Yumerefendi, J. E. Bear, B. Kuhlman, *Proc. Natl. Acad. Sci. USA* **2015**, *112*, 112.
[34] N. Srinivas, J. Parkin, G. Seelig, E. Winfree, D. Soloveichik, *Science* **2017**, *358*, 2052.
[35] L. Qian, E. Winfree, *Science* **2011**, *332*, 1196.
[36] G. Seelig, D. Soloveichik, D. Y. Zhang, E. Winfree, *Science* **2006**, *314*, 1585.
[37] L. Qian, E. Winfree, J. Bruck, *Nature* **2011**, *475*, 368.
[38] J. Steinkühler, R. L. Knorr, Z. Zhao, T. Bhatia, S. M. Bartelt, S. Wegner, R. Dimova, R. Lipowsky, *Nat. Commun.* **2020**, *11*, 905.
[39] D. Duguay, R. A. Foty, M. S. Steinberg, *Dev. Biol.* **2003**, *253*, 309.
[40] A. Oyler-Yaniv, J. Oyler-Yaniv, B. M. Whitlock, Z. Liu, R. N. Germain, M. Huse, G. Altan-Bonnet, O. Krichevsky, *Immunity* **2017**, *46*, 609.
[41] S. Sun, M. Li, F. Dong, S. Wang, L. Tian, S. Mann, *Small* **2016**, *12*, 1920.
[42] L. Aufinger, F. C. Simmel, *Angew. Chem., Int. Ed.* **2018**, *57*, 17245.
[43] A. M. Tayar, E. Karzbrun, V. Noireaux, R. H. Bar-Ziv, *Nat. Phys.* **2015**, *11*, 1037.
[44] L. Tian, M. Li, J. Liu, A. J. Patil, B. W. Drinkwater, S. Mann, *ACS Cent. Sci.* **2018**, *4*, 1551.